A SNARE-like mechanism mediates bacterial outer membrane exchange

Carolina Basurto De Santiago[1¶], Elias J. Topo[1¶], Pengbo Cao[2,3], Daniel Wall[2#] and Beiyan Nan[1#]

[1]Department of Biology, Texas A&M University, College Station TX 77843, USA

[2]Department of Molecular Biology, University of Wyoming, Laramie, WY 82071, USA

[3]Present address: School of Medicine, Westlake University, Hangzhou, China

Running title: OME molecular mechanism

[¶] C. B. D. S. and E, J. T. contributed equally to this work

#Address correspondence to Beiyan Nan, bnan@tamu.edu; and Daniel Wall, dwall2@uwyo.edu

Keywords: *Myxococcus xanthus*, single-particle microscopy, cell surface protein, outer membrane exchange, kin recognition, membrane fusion, fusogen

Abstract

Kin recognition, the ability to distinguish self from nonself at the cellular level is critical to multicellular life. *Myxococcus xanthus* is a multicellular bacterium that cooperates among genetically-related cells and reduces exploitation by nonkin through outer membrane exchange (OME) of common goods and toxins. The polymorphic cell surface receptor called TraA and its partner protein TraB mediate kin recognition by OME, but its molecular mechanism remains unknown. Here we show that TraAB induce OME by overcoming the repulsive interaction between cells. Using quantitative microscopy techniques, we determined that TraA and TraB form complexes at a 1:1 ratio and that as few as one intercellular TraAB-TraAB dimer is sufficient to induce OME. We visualized the OME of single protein particles between cells and revealed that OME depends on the free diffusion of outer membrane (OM) contents. Our findings suggest a mechanism that shows analogies to the eukaryotic soluble N-ethylmaleimide-sensitive factor attachment protein receptors (SNAREs), which mediate plasma membrane fusion. *M. xanthus* OME provides a novel pathway that leads to an underlying conserved mechanism for membrane fusion that is a foundation process for multicellularity.

30 **Introduction**

31 The ability to distinguish self from nonself at the cellular level is critical to multicellular life.
32 This process ensures that highly related or clonal cells interact cooperatively while excluding
33 unrelated cells, which are often detrimental to multicellularity. For organisms that build
34 multicellularity by aggregating cells from their environment, self/nonself-recognition, or kin
35 recognition, is of paramount importance for coalescing a cooperative kin collective.

36 Myxobacteria are a group of aggregative multicellular organisms that possess
37 known systems for distinguishing relatedness at the genus and species levels (Kroos *et*
38 *al.*, 2025). Specifically, *Myxococcus xanthus* uses the type VI secretion system (T6SS) and
39 outer membrane exchange (OME) for this purpose (Vassallo & Wall, 2019, Vassallo *et al.*,
40 2020, Gong *et al.*, 2018). The T6SS is used by many Gram-negative bacteria for various
41 types of social conflicts and virulence and is relatively well understood (Cherrak *et al.*,
42 2019). In contrast, OME is restricted to myxobacteria and is not as well studied.

43 OME self-recognition occurs through homotypic binding between adjacent cells,
44 mediated by their polymorphic cell surface receptor called TraA and its operonic partner,
45 TraB (Pathak *et al.*, 2013, Cao & Wall, 2017). Following cell-cell recognition, TraAB
46 catalyzes OME, which involves the bidirectional transfer of different outer membrane
47 proteins (OMPs) and lipids between cells (Nudleman *et al.*, 2005, Wall, 2014, Pathak *et al.*,
48 2012). This process is thought to occur by transient outer membrane (OM) fusion, where
49 TraAB acts as a fusogen on each interacting cell (Cao *et al.*, 2015, Cao & Wall, 2019a). The
50 TraA protein contains a signal peptide (SP), a variable domain (VD) responsible for
51 recognition specificity, a cysteine-rich repeat region that likely functions as a presentation
52 stalk for the VD, and a MYXO-CTERM sorting tag that is likely lipidated to anchor it to
53 the cell surface (Sah *et al.*, 2020, Guo *et al.*, 2025). TraB contains an SP, an OM β-barrel,
54 and an OmpA cell-wall-binding domain. Forward genetic screens suggest that TraAB are
55 the only proteins required for OME (Dey & Wall, 2014, Vassallo *et al.*, 2021).

56 OME serves two broad functions: mediating cooperation and discriminating
57 between cells (Sah & Wall, 2020). For cooperation, OME can rescue genetic defects in
58 recipient cells by transferring a wild-type protein from donor cells (Hodgkin & Kaiser,
59 1977, Pathak *et al.*, 2012). OME can also rescue lethal OM defects by transferring
60 lipopolysaccharides (LPS) from healthy donors (Vassallo & Wall, 2016). Additionally,
61 when individual cells coalesce into tissue-like assemblages, genetically identical cells can
62 have distinct life histories that result in different adaptations depending on their age
63 and/or microenvironment exposures. Here, OME facilitates the transition to
64 homogeneous and synchronized cell populations with respect to their OM components
65 (Cao & Wall, 2019b), thus facilitating cooperation. Finally, adaptive traits suited to
66 particular environments can be transferred to naïve siblings via OME (Subedi *et al.*, 2024),
67 thus preparing or adapting them against future stresses.
68 OME also functions to discriminate against nonkin. This occurs by the exchange of
69 dozens of polymorphic lipoprotein toxins that belong to six different families (Dey *et al.*,
70 2016, Vassallo *et al.*, 2017, Vassallo & Wall, 2019, Weltzer *et al.*, 2025). Therefore, when
71 partnering cells are clonal, they are not intoxicated because they express a cognate set of
72 immunity proteins, which themselves are not exchanged. In contrast, when nonclonal
73 cells fortuitously possess compatible TraA receptors, a second discrimination step occurs,
74 wherein cells are reciprocally poisoned because they lack a complete set of immunity
75 proteins. These steps result in an extremely high level of specificity for self-recognition,
76 ensuring that highly related collectives form for multicellular functions, such as fruiting
77 body development.
78 Membrane fusion plays a central role in many biological processes in eukaryotic
79 cells, but in bacteria there are few examples and little is known. Here, we sought to
80 address key questions about the molecular mechanism of OME. First, we sought to
81 understand the nature of TraAB multimeric complexes that form upon cell-cell contact
82 and OME engagement. Following the coalescing of receptors, these complexes are readily

83 visualized as foci when using functional fluorescent protein fusions to TraA or TraB.
84 However, the stoichiometry of the intercellular TraA junction and the intracellular TraAB
85 complexes remains unknown. Second, since client OME cargos do not contain specificity
86 factors for transfer, but must be diffusible in a fluid OM, we aimed to measure the fluidity
87 of *M. xanthus* OM. Third, do these foci junctions serve as conduits for the transfer of client
88 proteins, and what trajectories do these proteins follow upon OME? Using
89 photobleaching and single molecule tracking techniques, we addressed these questions
90 and proposed an updated model of OME in myxobacteria.

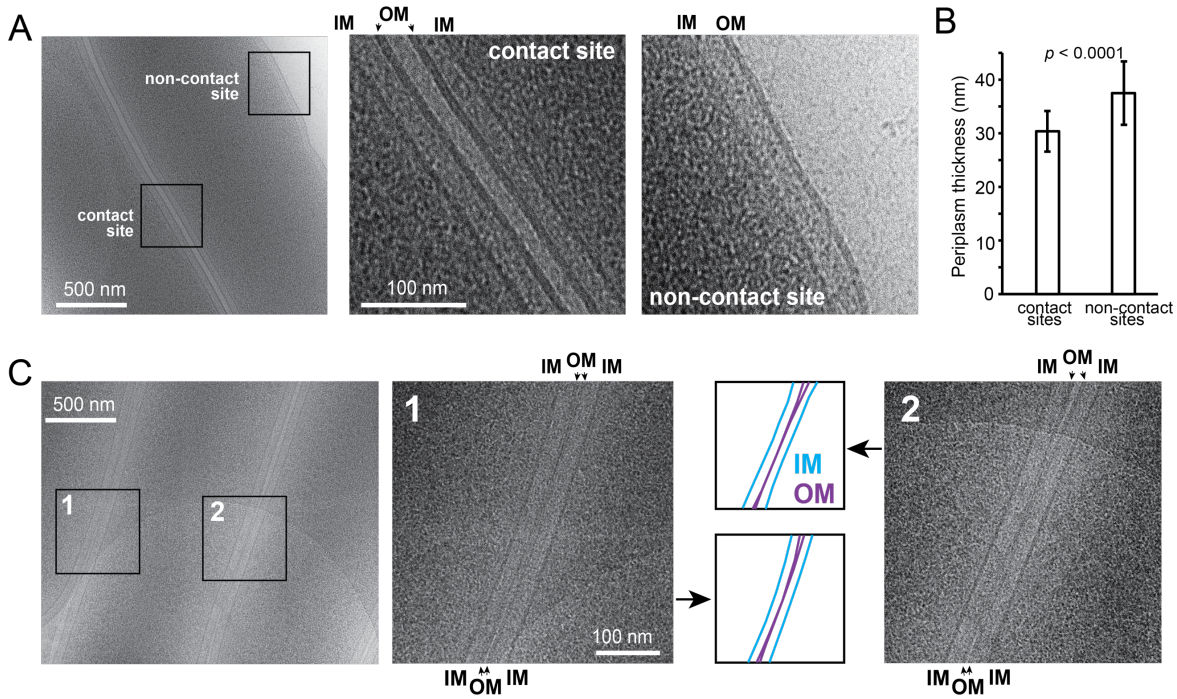

Fig. 1. TraAB facilitate OME by overcoming the repulsive interactions between cells. A) cryoEM images show that juxtaposed *pilA*⁻ cells do not make direct OM-OM contacts. In the same cell, the OM is relaxed at non-contact sites while stressed at cell-cell contact sites. **B)** Cell-cell contact induces stress compression of periplasms at contact sites. Periplasmic thickness was measured as the distance between the centers of the OM and IM densities from seven contacting cell pairs, 30 measurements/pair. The *p* value was calculated using a one-way ANOVA test between two unweighted, independent samples. **C)** Juxtaposed *pilA*⁻ cells that over produce TraAB frequently form direct OM-OM contacts that lead to OM fusion.

91 **Results**

92 **Repulsive interaction between cells obstructs OME**

93 Cells lacking functional TraAB or expressing incompatible TraA variants do not exchange

94 their OM contents (Wei *et al.*, 2011). This raises the question; why are TraAB required and
95 physical cell-cell contacts alone are insufficient for OM fusion? To answer this, we investigate
96 cell-cell contacts using cryogenic electron microscopy (cryoEM). To avoid the potential
97 interference from extracellular polysaccharides (EPS), we grew *pilA*$^{-}$ cells that do not
98 produce EPS (Yang *et al.*, 2010, Zhou & Nan, 2017) in liquid culture, concentrated cells by
99 centrifugation, and captured micrographs of *M. xanthus* cells in close contact, where we
100 found cell groups of various sizes. As OME does not occur in liquid, these cells displayed the
101 character of OMs before fusion (**Fig. 1A**).

102 Analyzing these micrographs, we found two remarkable features. First, regardless of
103 group size, physical interaction between OMs was not observed (**Fig. 1A**). The distances
104 between the centers of the OM densities at side-to-side cell contact sites varied between 20.4
105 nm and 34.5 nm, with an average distance of 28.8 ± 3.4 nm (measure from three pairs of cells,
106 30 measurements/pair). Therefore, the interaction between the OMs is under the regime of
107 electrostatic repulsion, likely driven by the strong negative charge on lipopolysaccharide
108 molecules, and beyond the range of van der Waals attraction, 0.3 – 0.5 nm (Batsanov, 2001).
109 Such repulsion is stronger than the one between weakly charged liposomes (3 – 10 nm
110 distance) that prevents their fusion in aqueous media (Jahn *et al.*, 2024). Hence juxtaposed
111 cells are always separated by a thin water layer and the repulsion between cells physically
112 obstructs OM fusion. Second, the periplasms appeared compressed at cell-cell contact sites
113 (**Fig. 1A**). Strikingly, in the cells that contact others only on one side, only the contact sides
114 displayed compressed periplasms with the thickness (the distance between the centers of the
115 OM and IM densities) of 30.4 ± 3.8 nm, while the non-contact sides retained relaxed
116 periplasms of 37.5 ± 5.9 nm thickness (measured from the same seven pairs of cells, 30
117 measurements/pair, for both measurements, **Fig. 1B**). This result shows that cell-cell contacts
118 increase the surface tension of OMs. Therefore, similar to plasma membranes that do not fuse
119 spontaneously (Rand & Parsegian, 1984), repulsion must be overcome to bring OMs closer,

120 which poses a major energy barrier in OM fusion.

121 **TraAB induce OME by overcoming the repulsive interaction between cells**

122 To visualize how TraAB facilitate OME, we subjected a *pilA*$^{-}$ strain that expressed *traAB*
123 ectopically by the strong *pilA* promoter (*traAB*^{OE}) (Pathak *et al*., 2012), to cryoEM imaging. In
124 stark contrast to its parent strain that maintained a nearly constant OM spacing (**Fig. 1A**), the
125 OM-OM distance between juxtaposed *traAB*^{OE} cells varied considerably. Notably, these cells
126 frequently made close OM contacts that often culminated in an apparent OM fusion-like
127 configuration (**Fig. 1C**). Hence, TraAB-TraAB complexes between cells overcomes repulsive
128 interactions between juxtaposed OMs and thus induces OME.

129 **Stoichiometry of the intercellular TraA foci**

130 TraAB are thought to function as fusogens to catalyze OM fusion between cells. By using
131 fluorescent fusion reporters to TraA or TraB they were found to coalesce into foci aggregates
132 upon cell-cell contact (Cao & Wall, 2019a). Here we sought to address (i) how many TraA
133 molecules are present in these foci? (ii) Do all the TraA foci contain the same stoichiometry,
134 and (iii) do interacting cells contribute the same number of TraA proteins in each focus? To
135 answer these questions, we used a functional monomeric super folder green fluorescent
136 protein (GFP)-labeled TraA (TraA-GFP) expressed from the heterologous *pilA* promoter and
137 placed it in a Δ*traA* strain (Cao & Wall, 2019a). We mixed this strain with wild-type
138 (unlabeled) cells at a 1:2 ratio and spotted the cell mixture on a 1.5% agar surface. As reported
139 (Cao & Wall, 2019a), TraA-GFP distributed uniformly throughout the OM of isolated cells.
140 However, upon cell-cell contact, we observed two types of TraA foci at contact junctions,
141 bright foci occurred between two labeled cells and dim foci between labeled and unlabeled
142 cells (**Fig. 2A**).

143 The intensities of TraA-GFP foci appeared heterogeneous, regardless of whether only
144 one or both cells were labeled (**Fig. 2A**), suggesting that individual TraA foci do not adopt
145 the same stoichiometry. We then subjected the TraA-GFP foci to photobleaching using a 488-

146 nm laser (0.5 kW/cm²) and monitored the decrease of fluorescent signals continuously at 67
147 Hz (15 ms/frame). The intensity of these foci decreased in discrete steps of the same size,
148 which we define as Δ*i* that reflected the photobleach of one GFP molecule (**Fig. 2B**).
149 Occasionally we saw larger bleach steps where the intensity decreased by 2Δ*i*, indicating that
150 two molecules were bleached simultaneously (**Fig. 2B**). Therefore, the number of Δ*i* bleach
151 steps equal the number of TraA-GFP molecules within the focus (**Fig. 2B, Movie S1**).

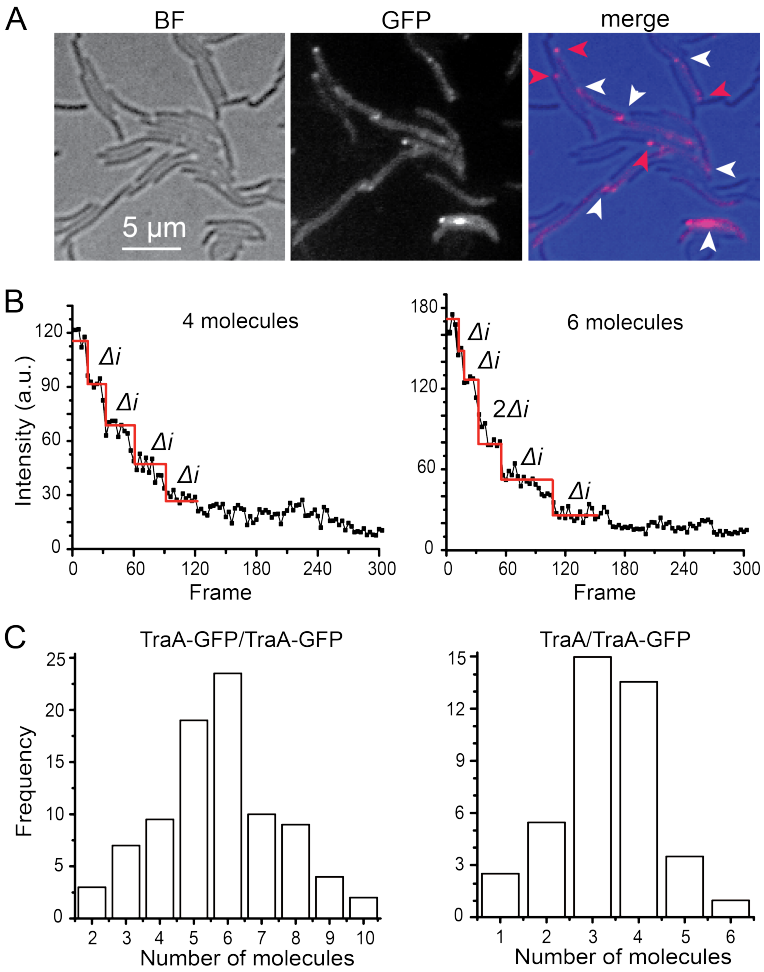

Fig. 2. TraA forms heterogeneous foci at cell-cell contact sites. **A)** Representative images of the TraA-GFP foci. The Δ*traA traA-gfp* cells were mixed with wild-type (unlabeled) at a 1:2 ratio. White arrows indicate foci formed between labeled cells and red arrows between labeled and unlabeled cells. **B)** Examples of the photobleached foci that contain 4 and 6 TraA-GFP molecules, respectively. The decrease step of fluorescence corresponds to one GFP molecule being photobleached (*Δi*). **C)** The number of TraA-GFP molecules in each focus between labeled cells (left, n = 87) and between labeled and unlabeled ones (right, n = 41).

152 Consistent with the variation of their fluorescent intensities, the 87 foci between labeled
153 cells lost fluorescence after 2 to 10 steps of photobleaching, indicating that these foci
154 contained 2 to 10 TraA-GFP molecules (**Fig. 2B, Movie S1**). The numbers of TraA-GFP
155 molecules in each focus displayed a typical Gaussian distribution. Importantly, we never
156 observed any foci that was bleached in a single step of Δ*i*, suggesting that at least one TraA
157 molecule in each juxtaposed cell was required to establish the intercellular junction. This
158 result was consistent with the observation that TraA-GFP expressing cells cannot form TraA
159 foci when it contacts a Δ*traA* cell (Cao & Wall, 2019a). In addition, 46% of these foci contained
160 odd numbers of TraA molecules, indicating that the formation of these foci does not
161 necessarily require the same number of TraA molecules from two juxtaposed cells.
162 Among the 41 foci found between labeled and unlabeled cells, the number of TraA-GFP
163 molecules also showed a nearly symmetric distribution between 1 and 6, roughly half as
164 many as detected in the foci between two labeled cells (**Fig. 2C**). The detection of foci that
165 contained only one TraA-GFP molecule further confirmed that a single TraA molecule from
166 each contacting cell was sufficient to establish an intercellular TraA junction. Taken together,
167 TraA foci at cell-cell contact sites contain molecules from both juxtaposed cells where each
168 cell may contribute different numbers of TraA molecules.

169 **TraA and TraB form complexes at a 1:1 ratio**

170 TraA requires its partner OMP TraB to form functional complexes (Pathak *et al.*, 2012, Cao &
171 Wall, 2017). Although TraB does not play a specificity role in kin recognition, TraA and TraB
172 colocalize into the foci between adjacent cells in an interdependent manner, suggesting that
173 these proteins form intracellular complexes (Cao & Wall, 2019a). However, the stoichiometry
174 of these complexes is unknown. To address this question, we used a strain that expressed
175 both TraA-mCherry and TraB-GFP and photobleached both mCherry and GFP
176 simultaneously using Hamamatsu W-VIEW GEMINI™ beam-splitter. TraA and TraB
177 colocalized in the foci between juxtaposed cells (**Fig. 3A**). To simplify analysis, we recorded

178 the photobleach of both fluorophores at 5 Hz (200 ms/frame, **Movie S2**). Using this method,
179 we found that the numbers of TraA-mCherry in each focus varied between 2 and 12 in the 59
180 analyzed foci (**Fig. 3B**), consistent with the photobleach result from TraA-GFP (**Fig. 2C**).
181 Importantly, the TraB-GFP molecules displayed a similar distribution pattern (**Fig. 3B**). We
182 further investigated the correlation between TraA and TraB in each focus and found that each
183 TraA molecule correlated with 0.98 TraB molecules, indicating that TraA and TraB form
184 complexes at a 1:1 ratio (**Fig. 3C**).

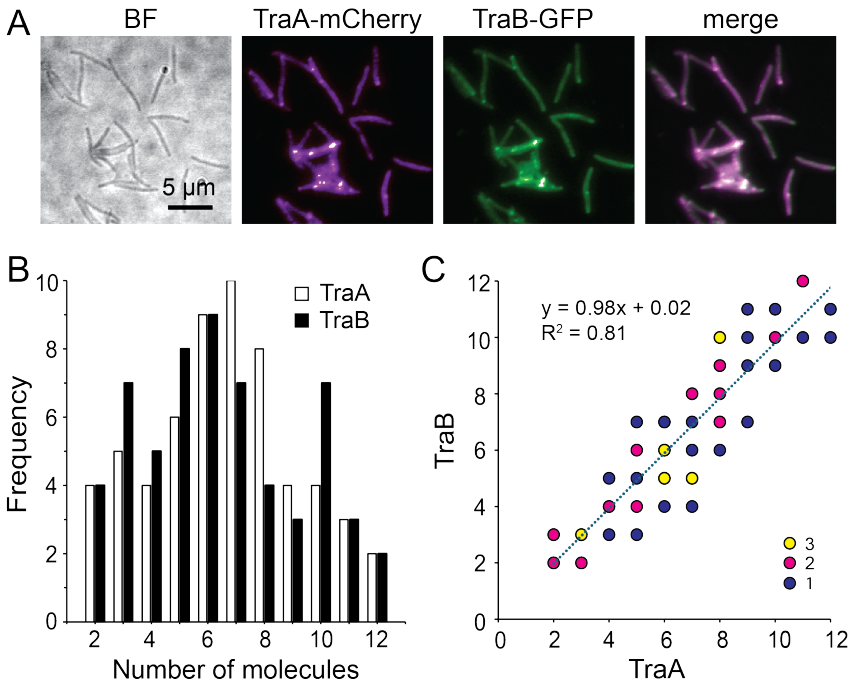

Fig. 3. TraA and TraB form intracellular complexes at a 1:1 ratio. **A)** TraA-mCherry and TraB-GFP colocalize in the foci between adjacent cells. **B)** From 59 foci analyzed, the number of TraA and TraB proteins in each focus show similar distribution patterns. **C)** The correlation between the numbers of TraA and TraB in individual foci suggests a 1:1 ratio in the intracellular TraAB complexes. In each focus, the number of TraB is plotted against that of TraA. The numbers of foci that have the same TraA:TraB ratio are indicated by color.

185 ***M. xanthus* contains a highly fluid OM**

186 The model bacterium *Escherichia coli* has a rigid OM (Rojas *et al.*, 2018, Sun *et al.*, 2022). As a
187 consequence, the lateral mobility of OMPs is restricted due to the formation of large OMP
188 islands and the selective presence of bulky LPS molecules in the outer leaflet (Rassam *et al.*,
189 2015, Benn *et al.*, 2021). In contrast, *M. xanthus* cells are flexible and can exchange a broad

190 range of OM molecules efficiently, including OMPs, LPS, and dyes (Ducret *et al.*, 2013,
191 Vassallo *et al.*, 2015, Pathak *et al.*, 2012). Since heterologous proteins, like a lipidated GFP, are
192 readily exchanged as cargos, OME does not require other *cis* specificity sequences for
193 transfer. Instead, these cargos are likely transferred between cells by diffusion, which
194 requires a fluid OM (Cao & Wall, 2020, Cao & Wall, 2019a). However, the fluidity of *M.*
195 *xanthus* OM has not been measured.

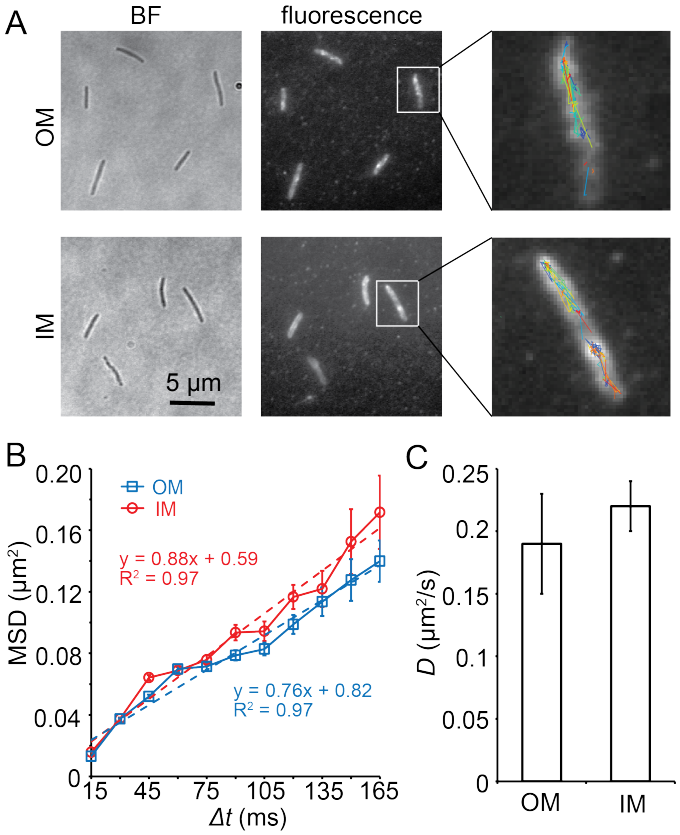

Fig. 4. SS_{OM}-PAmCherry diffuses rapidly in the *M. xanthus* OM. **A)** Single PAmCherry particles diffuse freely in both the OM and IM. The overall distribution of SS_{OM}- and SS_{IM}-PAmCherry is displayed using the composite of 100 consecutive frames taken at 15-ms intervals. Single-particle trajectories of PAmCherry were generated from the same frames. Individual trajectories are distinguished by colors. **B)** The linear relationship between MSD and Δ*t* indicates that PAmCherry diffuses freely in both OM (n = 674) and IM (n = 1276). **C)** PAmCherry shows similar diffusion coefficients in OM (n = 674) and IM (n = 1276).

196 To measure membrane fluidity, we used the diffusion rate of OMPs as a proxy. Here, we
197 used a lipoprotein where a type II signal sequence was fused to the fluorescent protein
198 mCherry and expressed as a recombinant SS_{OM}-mCherry reporter in *M. xanthus.* This simple
199 lipoprotein tag was sufficient for the OM localization of mCherry and enabled it to be

200 transferred by OME (Wei *et al.*, 2011). We reengineered this strain by replacing mCherry with
201 the photoactivatable mCherry (PAmCherry). mCherry and PAmCherry are of the same size
202 and share 95.8% protein sequence identity. We used a 405-nm excitation laser (0.2 kW/cm^2,
203 0.1 s) to activate the fluorescence of a few labeled SS$_{OM}$-PAmCherry particles randomly (here
204 we refer isolated fluorescence spots as single particles rather than "single molecules" because
205 each spot could contain more than one molecule, albeit only the fluorescence of one molecule
206 was activated). We imaged the activated particles at 67 Hz using a 561-nm laser with total
207 internal reflection fluorescence (TIRF) microscopy (Fu *et al.*, 2018, Nan *et al.*, 2015, Nan *et al.*,
208 2013, Pogue *et al.*, 2018, Ramirez Carbo *et al.*, 2024, Zhang *et al.*, 2020). Using this setting, only
209 a thin section of each cell close to the coverslip was illuminated, which included the cell
210 surface. To exclude the potential influence of cell-cell contact, we only analyzed the dynamics
211 of SS$_{OM}$-PAmCherry particles in isolated cells. Using single particle tracking photo-activated
212 localization microscopy (sptPALM), we identified 1,518 fluorescent particles that remained
213 in focus for 4 - 12 frames (0.4 - 1.2 s) and plotted their mean squared displacements (MSDs)
214 against time lag (Δt). The linear relationship between MSD and Δt indicated that single SS$_{OM}$-
215 PAmCherry particles moved by typical diffusion (**Fig. 4A, B, Movie S3**). The diffusion
216 coefficient (D) of the entire population was 0.19 ± 0.04 μm^2/s (n = 674, **Fig. 4C**), in the same
217 order of magnitude as the unrestricted diffusion of proteins in the cytoplasm, IM, and
218 periplasm in other bacteria, such as *E. coli* and *Bacillus subtilis* (Parry *et al.*, 2014, Lucena *et al.*,
219 2018, Tran *et al.*, 2024). Importantly, the diffusion of SS$_{OM}$-PAmCherry was about 10-fold
220 faster than the restricted diffusion of *M. xanthus* proteins in the IM and periplasm (Fu *et al.*,
221 2018, Nan *et al.*, 2013, Zhang *et al.*, 2023b, Ramirez Carbo *et al.*, 2024), suggesting that SS$_{OM}$-
222 PAmCherry diffuses with little restriction in the OM.

223 The bacterial IM is known to be fluid, where many proteins diffuse freely (Lucena *et al.*,
224 2018). As a control, we engineered a strain that localizes mCherry to the IM (SS$_{IM}$-mCherry)
225 (Wei *et al.*, 2011) by replacing mCherry with PAmCherry. As expected, we found that the
226 recombinant SS$_{IM}$-PAmCherry also diffused freely, with a D value of 0.22 ± 0.02 μm^2/s (n =

227 1276), close to that of SS$_{OM}$-PAmCherry (**Fig. 4, Move S4**). Taken together, like the IM, the
228 OM of *M. xanthus* is highly fluid and such fluidity provides the mechanistic foundation for
229 OME.

230 **OME depends on the diffusion of OM components**

231 OME between *M. xanthus* cells has been imaged in real-time (Ducret *et al.*, 2013, Cao & Wall,
232 2019a). However, the mechanism of OME is not fully understood. For instance, does OME
233 depend on the diffusion of the client cargos, or the exchange of large OM fragments? To
234 investigate the dynamics and trajectories of client proteins during OME, we visualized and
235 tracked single SS$_{OM}$-PAmCherry particles. If OME requires diffusion, then SS$_{OM}$-PAmCherry
236 particles should quickly travel between cells. Alternatively, if cells exchange bulk OM
237 fragments, the exchange of SS$_{OM}$-PAmCherry particles should be slow due to the size of such
238 fragments.

239 To test these possibilities, we used cells that expressed SS$_{OM}$-PAmCherry as donors and
240 Δ*traA* P$_{pilA}$-*traA-gfp* cells as recipients. We mixed these strains at a 1:1 ratio on a 1.5% agar
241 surface. To increase the chance of capturing OME, we first exposed cells under the 405-nm
242 laser for 2 s, where the majority of PAmCherry was photoactivated (Fu *et al.*, 2018). We then
243 excited the fluorescence of PAmCherry and GFP using the 561-nm and 488-nm lasers,
244 respectively, and imaged both channels simultaneously using the beam-splitter. As SS$_{OM}$-
245 PAmCherry particles moved rapidly (**Fig. 4**), we had to track their movements at a high frame
246 rate (67 Hz). For this reason, we could only image each field for a few seconds before the
247 reporters' photobleach (**Fig. 2**). In these short time windows, OME was rarely visualized.
248 Nevertheless, we captured OME of 39 SS$_{OM}$-PAmCherry particles (**Fig. 5A-C, Movie S5-S7**).
249 Their MSD showed a linear relationship with Δt, with a D value of 0.21 ± 0.07 μm^2/s (n = 39),
250 close to the intracellular diffusion rate of SS$_{OM}$-PAmCherry particles. These results indicate
251 that cell-cell contact does not hinder OMP diffusion, and that OME depends on the diffusion
252 of OM content, rather than the transfer of large OM fragments (**Fig. 5D**).

253 By closely tracking particle trajectories during OME, we found six cases where SS$_{OM}$-
254 PAmCherry particles transferred to recipient cells and then returned to the donors (**Fig. 5A,**
255 **Movie S5**). This observation was consistent with OME occurring bidirectionally, where
256 'recipients' can also act as donors. Strikingly, we identified five SS$_{OM}$-PAmCherry particles
257 being transferred between more than two cells. For instance, the particle shown in **Fig. 5B**

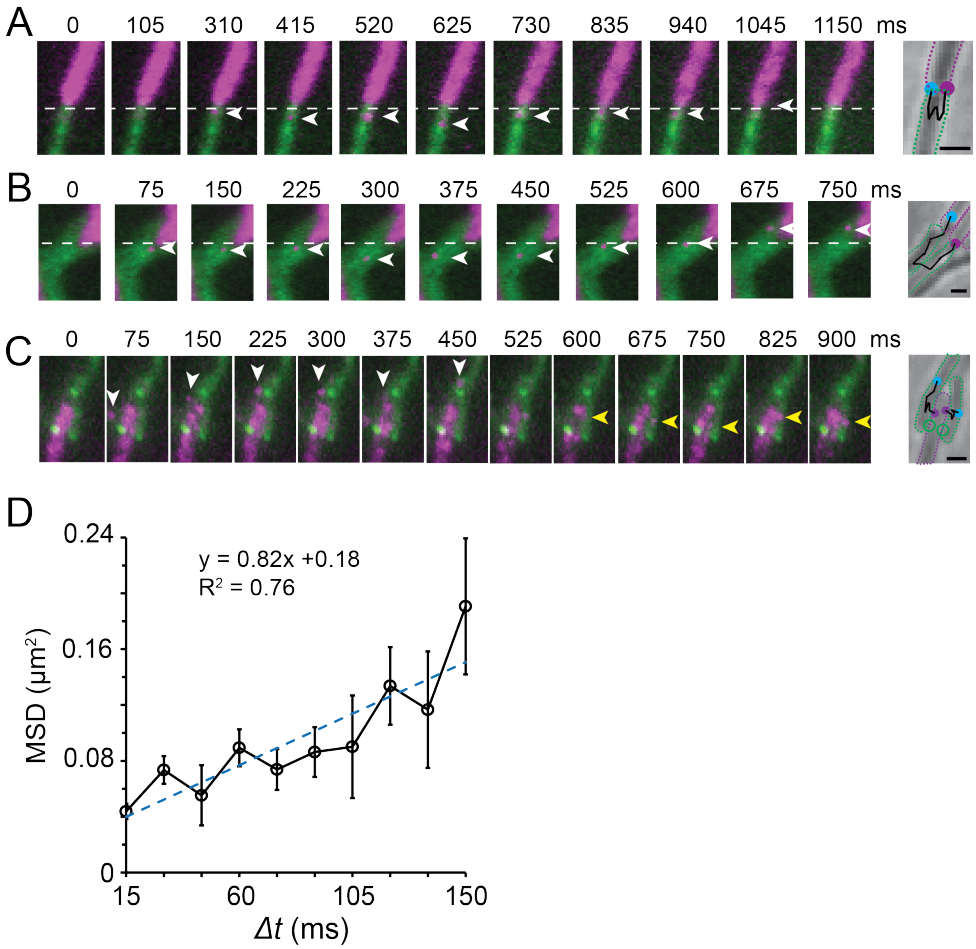

Fig. 5. OME requires cargo diffusion. **A - C)** Example trajectories of single SS$_{OM}$-PAmCherry particles during OME. The cells expressing SS$_{OM}$-PAmCherry (magenta) and TraA-GFP (green) were mixed at a 1:1 ratio. Arrows point to the exchanged particles. On the right side of each time-lapse series, the outlines of the donors and recipients are marked with purple and green dotted lines, respectively. The trajectories of particles are marked with black segmented lines. Their start and end positions are marked with purple and blue circles, respectively. Scale bars, 1 μm. The uncropped videos for these OME events are Movies S5, S6, and S7. In A) and B), the initial positions of the donor cell poles are marked with white dashed lines in the time-lapse images. In C), the positions of two TraA foci are marked with green circles on the right panel. **D)** The linear relationship between MSD and *Δt* of the 39 transferred particles indicates they diffuse freely during OME.

258 and **Movie S6** passed three cell-cell boundaries. Thus, through TraAB-mediated kin
259 recognition, client proteins can be serially transferred between clonemates to achieve long-
260 range OME among multiple adjacent cells.

261 **TraA foci do not correlate as the channels for OME**

262 Here we sought to investigate the role of TraAB complexes in OME and if they serve as
263 transfer portals. To answer these questions, we followed the trajectories of single-particle
264 OME events between cells that made lateral contacts. Such juxtaposed side-by-side cells
265 frequently formed multiple TraA foci, which allowed us to ask whether these foci correlated
266 as the sites where SS_{OM}-PAmCherry particles crossed the cell-cell boundaries. However, out
267 of the seven SS_{OM}-PAmCherry particles that transferred through lateral side-by-side cells,
268 none of them passed through the TraA foci (**Fig. 5C, Movie S7**). These observations strongly
269 suggest that TraAB complexes do not form transfer channels for OME.

270 **A SNAREs-like mechanism for TraAB-mediated OM fusion**

271 To understand how one intercellular TraAB-TraAB dimer induces OM fusion, we used
272 AlphaFold (Jumper *et al.*, 2021) to predict the structures of TraA and TraB. Using the
273 sequences of the processed proteins (amino acids 37 – 684 for TraA, excluding its SP and the
274 cleaved MYXO-CTERM (Sah *et al.*, 2020) and 23 – 543 for TraB, excluding its SP), AlphaFold
275 generated highly-confident structure models for both proteins in their monomeric states (**Fig.**
276 **6A**). TraA monomer forms a dumbbell-like structure where the N-terminal VD, containing
277 at least eight β-sheets, forms the first dumbbell head. The shaft is an extended cysteine-rich
278 region, which makes a 180° turn at the end, forming the second dumbbell head (**Fig. 6A**). This
279 region, containing more than 70 cysteines, forms at least eight β-hairpins that each consists
280 of two antiparallel β-strand connected by a short loop (**Fig. 6A**). We predict that at cell
281 surfaces where thiol groups are oxidized, this region is stiffened by dozens of disulfide
282 bonds. Consistent with a previous finding that the VD determines the recognition between
283 TraA variants (Cao & Wall, 2017), the AlphaFold structure showed two TraA molecules

interacting through their VDs, forming a head-to-head dimer (**Fig. 6A**). Strikingly, the length of a TraA dimer is ~ 28 nm, matching the distance between OMs in tightly packed cell groups (**Fig. 1A**).

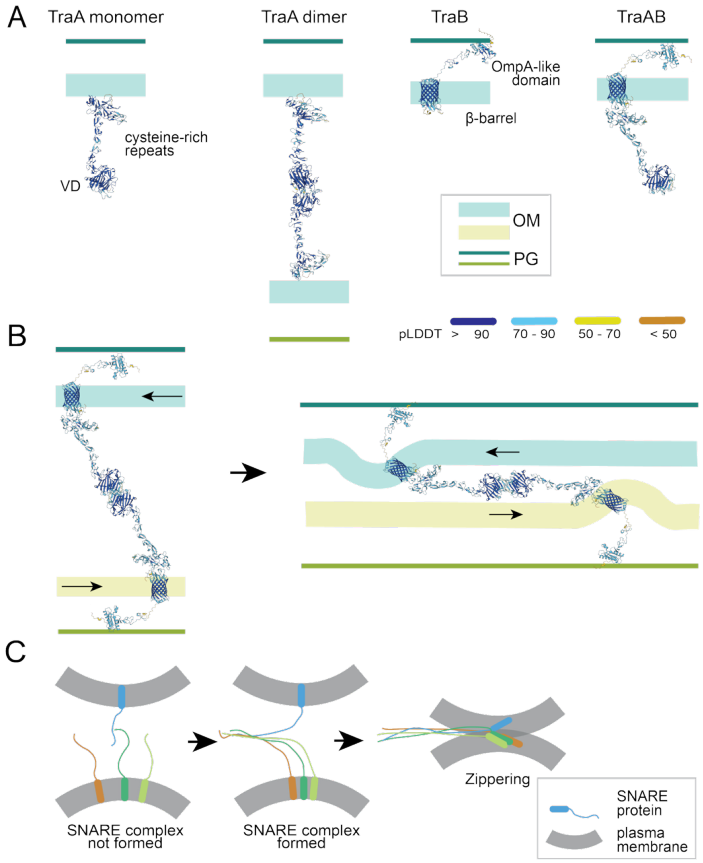

Fig. 6. Predicted structures of TraA, TraB, and their complexes suggest a mechanism for OM fusion comparable to the eukaryotic SNARE system. **A)** The predicted structures of TraA, TraB, and their complex. Structure elements are colored according to their pLDDT (predicted local-distance difference test) scores, which indicate the prediction confidence. **B)** A proposed bulge-and-slide mechanism for TraAB-mediated OM fusion. When two cells with compatible TraA molecules make contact, TraA molecules form head-to-head dimers, first through their VDs, and then TraB anchors such TraA dimers to PG. As the juxtaposed cells slide against each other, the two TraAB complexes move in opposite directions, pulling the OMs. Such mechanical stress will bring the OMs of adjacent cells closer and thus trigger OME. **C)** A model of SNARE-mediated plasma membrane fusion in eukaryotic cells. Assembly of SNAREs requires four different SNARE motifs on three or four separate proteins. Once a SNARE complex forms, the four coiled-coil domains transform into a four-helix bundle that "zips" the two membranes together.

The TraB protein consists of a N-terminal β-barrel and a C-terminal OmpA-like domain, linked together by short thrombospondin type 3 (TSP3) repeats predicted to bind calcium (Dai *et al.*, 2017) (**Fig. 6A**). Consistent with their colocalization and 1:1 stoichiometry (**Fig. 3**),

290 AlphaFold also predicted a 1:1 TraAB complex in which the second dumbbell head of TraA
291 is positioned on top of the β-barrel in TraB (**Fig. 6A**). However, AlphaFold did not predict
292 significant conformational changes in TraA after its dimerization and interaction with TraB
293 (**Fig. 6A**). Nevertheless, because TraB is diffusive in isolated cells but colocalizes with TraA
294 in the relatively stationary intercellular foci (Cao & Wall, 2019a), TraA dimerization could
295 introduce conformational changes in TraB, which then promotes binding to peptidoglycan
296 (PG) and thus restrains the diffusion of the TraAB-TraAB dimers.

297 Based on these predictions and our findings, we propose a model for TraAB-mediated
298 OM fusion that has similarities to the eukaryotic soluble N-ethylmaleimide-sensitive factor
299 attachment protein receptors (SNAREs) that mediate vesicle membrane fusion. To facilitate
300 fusion, membranes must be brought close together, and one way to do this is to minimize
301 their contact area. Eukaryotes utilize membrane-anchored SNARE proteins to establish
302 point-to-point contacts that perturb the bilayer structure and thereby lower the energy barrier
303 for fusion. Once SNARE proteins from juxtaposed membranes establish contact, the SNARE
304 complex tighten their coiled-coil domains into bundles, mimicking a zipper that pulls the
305 membranes together until they merge (Jahn *et al.*, 2024) (**Fig. 6D**). Through this mechanism,
306 one to three SNARE complexes are sufficient to catalyze membrane fusion (Jahn *et al.*, 2024,
307 Sinha *et al.*, 2011, Shi *et al.*, 2012, van den Bogaart *et al.*, 2010). Similarly, we propose that when
308 two cells that express compatible TraA variants approach each other, TraA molecules
309 establish point-to-point contacts between them. Diffusing TraA molecules can then form
310 intercellular dimers in a head-to-head orientation, which is consistent with TraA foci
311 formation between topologically opposed OMs. The TraAB complexes could anchor to PG
312 through the OmpA domain in TraB and thus forms relatively stationary junction foci like
313 SNARE complexes (**Fig. 6B**). While the TraA molecules in a dimer are not likely to form
314 SNARE-like zippers (**Fig. 6D**), when juxtaposed cells slide against each other, the movements
315 of cells pull the PG-anchored TraAB complexes toward opposite directions that tugs on the
316 OM and generates bulges at the base of each complex (**Fig. 6B**). As the cells continue to slide,

317 due to the rigidity of TraA, such stressed OM bulges are primed for membrane fusion as they
318 are forced into juxtaposed OMs, resulting in OM fusion between cells (**Fig. 6B**). In agreement
319 with our model, transmission electron microscopy (TEM) of cryo-fixed thin sections showed
320 that cells overexpressing TraAB contacted each other through OM bulges (Vassallo *et al.*, 2015)
321 (**Fig. 6C**).

322 **Discussion**

323 Multicellular organisms independently evolved from unicellular ancestors at least 25 times
324 during evolution (Grosberg & Strathmann, 2007). Myxobacteria achieve multicellularity
325 through the aggregation of single cells (Kroos *et al.*, 2025). While forming aggregates is
326 relatively straightforward, it is less understood how individual cells from genetically mixed
327 populations establish stable multicellular structures. For instance, how do individual cells
328 maintain cooperative cell-cell interactions while keeping cheaters at bay (Velicer *et al.*, 2000)?
329 Myxobacteria achieve the transition from solitary, single-cell life into cooperative,
330 multicellular tissues through kin recognition and the exchange of cellular contents (Sah &
331 Wall, 2020). Specifically, the homotypic binding by their polymorphic cell surface TraA
332 protein and its cohort protein TraB, leads to OM content sharing and further discrimination
333 against nonself by OME of polymorphic toxins. To better understand the mechanism of OME
334 we used quantitative microscopy and single molecule tracking. We showed that the ratio of
335 TraA and TraB in cell-cell junctions is 1:1. Moreover, we showed that overexpression of the
336 chromosomal copy of the *traAB* operon generates TraA foci of various stoichiometry, ranging
337 from 2 to 12. Our results confirmed that each partnering cell contributes at least one TraAB
338 complex to form a functional junction. Because the native, low expression of *traAB* is
339 sufficient for OME (Wei *et al.*, 2011), we postulate that the minimum number of TraAB
340 complexes in junctions for OME is two. Indeed, the foci that contained two TraAB complexes
341 only accounted for ~5% of all the foci we detected, which explains why such foci were hard
342 to image when TraAB were expressed with the native promoter (Cao & Wall, 2019a, Vassallo

343 *et al.*, 2015). Thus, overexpression increased both the number and size of such foci. The wide
344 range of stoichiometry and the fact that two partnering cells do not necessarily contribute
345 equal numbers of TraAB proteins in foci junctions, suggest that TraAB do not form
346 intercellular protein channels with defined structures.

347 Instead, our results invoke TraAB serving as fusogens to transiently catalyze the OM
348 fusion between cells and thus allow rapid and facile cargo exchange. This model presumes
349 that the OM of *M. xanthus* is fluid, distinct from the rigid OMs from other Gram-negative
350 bacteria such as *E. coli* (Cao & Wall, 2020). By tracking single molecules of the lipidated SS$_{OM}$-
351 PAmCherry, we showed this reporter rapidly diffuses in the OM. This analysis thus
352 confirmed *M. xanthus* OM fluidity, showing that diffusion rates in the OM were similar to
353 unrestricted protein diffusion rates in the cytoplasm, IM, and periplasm in other bacteria. It
354 is unclear how widely such fluid OMs exist in Gram-negative bacteria. Nevertheless, our
355 method can be easily applied to measure OM fluidity in other organisms.

356 Further support of the membrane fusion comes from tracking OME at single-particle
357 resolution. Here SS$_{OM}$-PAmCherry particles were observed to transfer from donor into
358 recipient cells at rates that are nearly identical to their diffusion rates. Strikingly, particles
359 were also observed to enter recipient cells and then return to the original donor, supporting
360 prior observations of bidirectional transfer mediated by OM fusion (Cao & Wall, 2019a).
361 Finally, in tracking experiments, particles also traveled across multiple cell boundaries when
362 those cells were adjacent to one another. This result indicates that multiple cells can
363 simultaneously form fusion junctions, which are in a tissue-like state. This latter point is also
364 supported by prior findings of serial cell-cell transfer of SitA toxins (Vassallo *et al.*, 2017).

365 The last question we addressed is whether TraAB foci serve as transfer portals for
366 OME. However, our observations did not find a correlation between TraA foci and single
367 particle transfer of the SS$_{OM}$-PAmCherry reporter. Instead, transfer occurs at various sites
368 along juxtaposed cells, which are not directly correlated with TraAB foci. Given these
369 findings, we propose TraAB foci serve as sites to nucleate membrane fusion. Once

370 "handshake" recognition occurs between TraAB complexes of juxtaposed cells, a small slide
371 or movement between cells is sufficient to bring the OMs together by pulling forces that
372 generate bulges on OMs, as observed in TEM micrographs of cell cross-sections (Vassallo *et*
373 *al.*, 2015). Additionally, fluorescent time-lapse microscopy of gliding *M. xanthus* cells engaged
374 in OME shows the functional TraA-mCherry reporter dynamically coalescing in a zipper-like
375 fashion along the lengths of the interacting cells (Cao & Wall, 2019a). Taken together, we
376 envision TraAB initiating an OM fusion junction that widens along the cell length. Fission
377 occurs when cells move apart from one another.

378 The outer leaflet of the *M. xanthus* OM contains LPS, consisting of the lipid A membrane
379 anchor and extended aqueous exposed polysaccharide O-antigen repeats (Perez-Burgos *et al.*,
380 2019). Additional types of lipids may also reside in their outer leaflet, but that is not fully
381 understood (Lorenzen *et al.*, 2014). Since TraAB has no known connection to the IM or
382 cytoplasmic energy sources, we propose that when cells slide against each other, the
383 mechanical force of cell movements, an essential requirement for OME (Wei *et al.*, 2011),
384 could pull OMs outward through the rigid TraAB-TraAB dimer and eventually cause OM
385 fusion (**Fig. 6B**). Our model shows similarities to the eukaryotic SNARE mechanism in how
386 membranes are brought together to overcome the energy barrier that obstructs membrane
387 fusion (**Fig. 6D**). However, in contrast to the SNARE complexes that require four SNARE
388 motifs from three to four proteins, the TraAB-TraAB dimer is simpler but contains the same
389 essential structural elements: the interaction domains in TraA and the membrane anchor in
390 TraA and TraB (**Fig. 6A**). Different from the SNARE complexes, which pull membranes
391 together through large-scale conformational changes (**Fig. 6D**), the energy for bringing
392 membranes in proximity comes from sliding movements between cells by either motility or
393 cell growth (**Fig. 6B**). Nevertheless, we do not rule out the possibility that conformational
394 changes in TraA could also play important roles in OM fusion. In this regard, a candidate
395 conformational switch within the diverse TraA family is the invariant Ser-Cys-Asn-Cys-Cys-
396 Pro motif found in the C-terminal stalk region (Cao *et al.*, 2019). Here the adjacent Cys

397 residues may form a sterically constrained disulfide bond that brakes upon tension by TraA-
398 TraA receptors adhering as cells move in opposite directions.

399 Our model explains two important observations. First, whereas TraA and TraB do not
400 depend on each other to localize to OMs, their function as cell-cell adhesins and for the
401 formation of junction foci requires both proteins. In this case, TraA is required for kin
402 recognition through its VD to initiate intercellular dimer formation, while TraB is essential to
403 anchor such dimers to PG and to restrain their diffusion. This latter point is supported by the
404 finding that deletion of the OmpA domain from TraB results in a truncated protein able to
405 form foci and act as an adhesion with TraA, but is not functional for OME (Balagam *et al.*,
406 2021). Second, OME requires cell motility (Wall *et al.*, 1998, Wall & Kaiser, 1998, Wei *et al.*,
407 2011). Our model predicts that the relative movements pull on OMs through the rigid TraA-
408 TraA dimers, and such mechanical stress will produce pronounced OM bulges that forces
409 OMs together, while also perturbing the bilayer structure, and thereby lowering the energy
410 barrier to the point where fusion occurs spontaneously (**Fig. 6B**). Our model further predicts
411 that after fusion, fission occurs when cells move apart from each other, where long narrow
412 OM tubes are sometimes seen between separating cells (Ducret *et al.*, 2013, Wei *et al.*, 2014).
413 In future studies, it will be interesting to test if exogenous expression of TraAB in other
414 bacteria with fluid OMs facilitates OME. However, there are technical issues reconstituting
415 the MYXO-CTERM sorting pathway for TraA cell surface localization in a heterologous host
416 (Sah *et al.*, 2020, Guo *et al.*, 2025). Nevertheless, if successful, this method can be used in
417 synthetic biology for generating bacterial multicellular structures.

418 **Materials and methods**

419 **Bacterial strains, plasmids and growth conditions**

420 Vegetative *M. xanthus* cells were grown in liquid CYE medium (10 mM MOPS pH 7.6, 1%
421 (w/v) Bacto™ casitone (BD Biosciences), 0.5% yeast extract and 8 mM $MgSO_4$) at 32 °C, in
422 125-ml flasks with vigorous shaking, or on CYE plates that contains 1.5% agar. Strains,

423 plasmids, and primers used in this study are listed in Supplementary **Table 1**. To create
424 P_{pilA}-*SS*$_{OM}$-*PAmCherry* (pPC60), fragments of P_{pilA}-*SS*$_{OM}$ and *PAmCherry* were PCR
425 amplified (Q5, New England Biolabs), and the resulting amplicons containing 25 bp
426 overhangs were ligated into the pSWU19 vector (linearized with EcoRI and XbaI) in
427 Gibson Assembly Master Mix (New England Biolabs). Construction of the SS_{IM}–
428 PAmCherry fusion was done following the published method (Wei *et al.*, 2011). This
429 construct was made by PCR amplification of genomic DNA with primers P_{pilA}-F2 and
430 SS_{IM}–mCherry-R (**Table 1**). The 5′ tail of the latter primer encodes 81 bp from MXAN_1176
431 that encode the N-terminal IM localization signal plus the downstream 10 amino acids
432 (CKDSDKKESM) for IM retention (Wei *et al.*, 2011). This PCR product was cloned to the
433 5′ end of PAmCherry at the XbaI site. Plasmids were verified by PCR, restriction enzyme
434 digestion, and if necessary, DNA sequencing. Verified plasmids were then electroporated
435 into *M. xanthus* cells and selected with appropriate antibiotics. The strains, plasmids and
436 primers used in this study are listed in **Table 1**.

437 **Table 1. Strains, plasmids, and primers used in this study.**

Strain name	Description	Source
DZ4469	DZ2 *pilA::tet*, Tc^R	(Vlamakis *et al.*, 2004)
DW1463	DK8601 (*aglQ1 pil*A::*tet*) *PpilA-traAB*, Tc^R	(Pathak *et al.*, 2012)
DW1483	DK8601 (*aglQ1 pil*A::*tet*) Δ*traAB*, Tc^R	(Cao & Wall, 2017)
DW2279	DW1483 pPC44, Km^R, Tc^R	(Cao & Wall, 2019a)
DW2285	DW1483 pPC49, Km^R, Tc^R	(Cao & Wall, 2019a)
DW2302	DW8601 pPC60 Km^R, Tc^R	This study
BN360	DW8601 pBN-IMPAC Km^R, Tc^R	This study

Plasmid name	Description	Source
pPC60	P_{pilA}-*SS*$_{OM}$-*PAmCherry* in pSWU19, Km^R	This study
pPC41	P_{pilA}-*traA-gfp-traB* in pSWU19, Km^R	(Cao & Wall, 2019a)
pPC44	P_{pilA}-*traA-mCherry-traB* in pSWU19, Km^R	(Cao & Wall, 2019a)
pPC49	P_{pilA}-*traA-traB-gfp* in pSWU19, Km^R	(Cao & Wall, 2019a)
pBN-IMPAC	P_{pilA}-*SS*$_{IM}$-*PAmCherry* in pSWU19, Km^R	This study

Primer name	Sequence (from 5' to 3')	Use
pSWU19-EcoRI-P_{pilA}-F	AGGAAACAGCTATGACCATGATTACGAATTCCGTCATGTTGGACGAGGT	pPC60
P_{pilA}-*SS*$_{OM}$-*PAmCherry*-R	GCCCTTGCTCACTCTAGAAGGAAACGAGCAACCG	pPC60
P_{pilA}-*SS*$_{OM}$-*PAmCherry*-F	GTTTCCTTCTAGAGTGAGCAAGGGCGAGGAG	pPC60
PAmCherry-XbaI-R	TGCATGCCTGCAGGTCGACTCTAGAAAGCTTTTACTTGTACAGCTCGTCCATGC	pPC60

P_{pilA}-F2	GGATCTAGATGCATGCGGCCGCGTCATGTTGGACGAGGTC	pBN-IMPAC
SS_{IM}-mCherry-R	CACATCTAGACATGGATTCCTTCTTGTCGGAGTCCTTGCAGG CGGTGAGGGTAAGGCAGAGGAGGACAGTCGTCAGGAATTG GGTCCGCATGGTGACTCTCCTCCGGGGGTCCTCAGAGAAG GTTG	pBN-IMPAC

438 **Light microscopy and image analysis**

439 For all imaging experiments, 5 ml cells or cell mixtures were spotted on a 1.5% (w/v) agar
440 pad containing 10 mM MOPS pH 7.6 and 8 mM $MgSO_4$. All microscopy images were
441 captured using an Andor iXon Ultra 897 EMCCD camera (effective pixel size 160 nm) on an
442 inverted Nikon Eclipse-Ti™ microscope with a 100× 1.49 NA TIRF objective. GFP and
443 mCherry were photobleached using the 488-nm and 561-nm lasers (0.5 kW/cm^2), respectively
444 at the stated frame rates. sptPALM was performed as previously described (Fu *et al.*, 2018).
445 *M. xanthus* cells were grown in CYE to OD_{600} around 1. PAmCherry was activated using a
446 405-nm laser (0.3 kW/cm^2), excited and imaged using a 561-nm laser (0.2 kW/cm^2). Images
447 were acquired at 67 Hz (15 ms/frame). For each sptPALM experiment, single PAmCherry
448 particles were localized in at least 100 individual cells from three biological replicates.
449 sptPALM and cell morphology data were analyzed as previously described using a MATLAB
450 (MathWorks) script (Fu *et al.*, 2018, Zhang *et al.*, 2023a, Zhang *et al.*, 2023b). Briefly, cells were
451 identified using differential interference contrast images. Single PAmCherry particles inside
452 of cells were fitted by a symmetric 2D Gaussian function; its center was assumed to be the
453 particle's position (Fu *et al.*, 2018). Particles in consecutive frames were considered to belong
454 to the same trajectory when they were within a user-defined distance of 320 nm (two pixels).
455 Sample trajectories were generated using the TrackMate plugin (Ershov *et al.*, 2022) in the
456 ImageJ suite (https://imagej.net). For simplicity, we considered all the mobile particles of
457 these proteins displaying typical diffusion and determined their D from a linear fit to the first
458 four points of the MSD using a simpler formula MSD = $4D\Delta t$ (Fu *et al.*, 2018, Lee *et al.*, 2016).
459 Error bars were the standard derivation of 1,000 bootstrap samples using the published
460 method (Morgenstein *et al.*, 2015).

461 **Cryo-EM**

462 Bacterial strains were grown overnight in CYE media with appropriate antibiotics,
463 incubated with shaking at 32 °C and 250 rpm to an optical density of OD_{600} 0.6. Cells were
464 collected by centrifugation at 5,000 rpm and room temperature for 3 min and
465 resuspended in CYE media to a final OD_{600} of 12. The cell suspension (3 µl) was applied
466 to C Flat-1.2/1.3 200 mesh copper grids (Electron Microscopy Sciences) that were glow
467 discharged for 30 s at 15 mA. Grids were plunge-frozen in liquid ethane with an FEI
468 Vitrobot Mark IV (Thermo Fisher Scientific) at 4 °C, 100% humidity with a waiting time
469 of 30 s, two-side blotting time of 2.5 - 3 s, and blotting force of 0. All subsequent grid
470 handling and transfers were performed in liquid nitrogen. Grids were clipped onto cryo-
471 FIB autogrids (Thermo Fisher Scientific). We used a Titan Krios G4 transmission electron
472 microscope (Thermo Fisher Scientific), equipped with a Gatan K3 direct electron detector
473 and a Gatan BioContinuum energy filter. Imaging was performed using a 15 eV slit width
474 on the energy filter to enhance image contrast. Micrographs were recorded in counted
475 mode at a nominal magnification of 30,000 x, using a dose rate of 14.65
476 electrons/pixel/second over a 2.6-second exposure, resulting in a total accumulated dose
477 of 50 electrons/$Å^2$. Low magnification images were taken at 6500 x with a pixel size of
478 1.39 nm.

Acknowledgments

This work was supported by the National Institutes of Health grants GM129000 to B. N. and GM140886 to D.W.

Movie captions

Movie S1. TraA-GFP foci being photobleached. Time-lapse images were recorded at 67 Hz and played at the same frame rate (real time).

Movie S2. Simultaneous photobleaching of TraA-mCherry (right) and TraB-GFP (left) in foci between adjacent cells. Time-lapse images were recorded at 5 Hz and played at the same frame rate (real time).

Movie S3. Diffusion of OMss-PAmCherry particles. Time-lapse images were recorded at 67 Hz and played at the same frame rate (real time).

Movie S4. Diffusion of IMss-PAmCherry particles. Time-lapse images were recorded at 67 Hz and played at the same frame rate (real time).

Movie S5. OME is bidirectional. The donor cell expresses OMss-PAmCherry (magenta) and the recipient TraA-GFP (green). The particle was first transferred to the recipient and then returned to the donor. Time-lapse images were recorded at 67 Hz and played at 7 frames/s, about 1/10 speed of real time.

Movie S6. Serial cell-cell transfer of OMss-PAmCherry particle by OME. Donor cell expresses OMss-PAmCherry (magenta) and the recipients TraA-GFP (green). Particle was serially transferred, crossing three cell-cell boundaries. Time-lapse images were recorded at 67 Hz and played at 7 frames/s, about 1/10 speed of real time.

Movie S6. TraAB foci do not function as OME conduits. Donor cell expresses OMss-PAmCherry (magenta) and the recipients TraA-GFP (green). Two OMss-PAmCherry particles transferred across cell boundaries, but not through the TraAB foci. Time-lapse images were recorded at 67 Hz and played at 7 frames/s, about 1/10 speed of real time.

References

Balagam, R., Cao, P., Sah, G.P., Zhang, Z., Subedi, K., Wall, D., and Igoshin, O.A. (2021) Emergent myxobacterial behaviors arise from reversal suppression induced by kin contacts. *mSystems* **6**: e0072021.

Batsanov, S.S. (2001) Van der Waals Radii of Elements. *Inorganic Materials* **37**: 871-885.

Benn, G., Mikheyeva, I.V., Inns, P.G., Forster, J.C., Ojkic, N., Bortolini, C., Ryadnov, M.G., Kleanthous, C., Silhavy, T.J., and Hoogenboom, B.W. (2021) Phase separation in the outer membrane of *Escherichia coli*. *Proc Natl Acad Sci U S A* **118**.

Cao, P., Dey, A., Vassallo, C.N., and Wall, D. (2015) How myxobacteria cooperate. *J Mol Biol* **427**: 3709-3721.

Cao, P., and Wall, D. (2017) Self-identity reprogrammed by a single residue switch in a cell surface receptor of a social bacterium. *Proc Natl Acad Sci U S A* **114**: 3732-3737.

Cao, P., and Wall, D. (2019a) Direct visualization of a molecular handshake that governs kin recognition and tissue formation in myxobacteria. *Nature communications* **10**: 3073.

Cao, P., and Wall, D. (2020) The Fluidity of the Bacterial Outer Membrane Is Species Specific: Bacterial Lifestyles and the Emergence of a Fluid Outer Membrane. *Bioessays* **42**: e1900246.

Cao, P., Wei, X., Awal, R.P., Muller, R., and Wall, D. (2019) A highly polymorphic receptor governs many distinct self-recognition types within the *Myxococcales* order. *mBio* **10**: 10.1128/mbio.02751-02718.

Cao, P.B., and Wall, D. (2019b) Direct visualization of a molecular handshake that governs kin recognition and tissue formation in myxobacteria. *Nat Commun* **10**.

Cherrak, Y., Flaugnatti, N., Durand, E., Journet, L., and Cascales, E. (2019) Structure and Activity of the Type VI Secretion System. *Microbiol Spectr* **7**.

Dai, S., Sun, C., Tan, K., Ye, S., and Zhang, R. (2017) Structure of thrombospondin type 3 repeats in bacterial outer membrane protein A reveals its intra-repeat disulfide bond-dependent calcium-binding capability. *Cell Calcium* **66**: 78-89.

Dey, A., Vassallo, C.N., Conklin, A.C., Pathak, D.T., Troselj, V., and Wall, D. (2016) Sibling Rivalry in *Myxococcus xanthus* Is Mediated by Kin Recognition and a Polyploid Prophage. *Journal of Bacteriology* **198**: 994-1004.

Dey, A., and Wall, D. (2014) A genetic screen in *Myxococcus xanthus* identifies mutants that uncouple outer membrane exchange from a downstream cellular response. *J Bacteriol* **196**: 4324-4332.

Ducret, A., Fleuchot, B., Bergam, P., and Mignot, T. (2013) Direct live imaging of cell-cell protein transfer by transient outer membrane fusion in *Myxococcus xanthus*. *Elife* **2**: e00868.

Ershov, D., Phan, M.S., Pylvanainen, J.W., Rigaud, S.U., Le Blanc, L., Charles-Orszag, A., Conway, J.R.W., Laine, R.F., Roy, N.H., Bonazzi, D., Dumenil, G., Jacquemet, G., and Tinevez, J.Y. (2022) TrackMate 7: integrating state-of-the-art segmentation algorithms into tracking pipelines. *Nat Methods* **19**: 829-832.

Fu, G., Bandaria, J.N., Le Gall, A.V., Fan, X., Yildiz, A., Mignot, T., Zusman, D.R., and Nan, B. (2018) MotAB-like machinery drives the movement of MreB filaments during bacterial gliding motility. *Proc Natl Acad Sci U S A* **115**: 2484-2489.

Gong, Y., Zhang, Z., Zhou, X.W., Anwar, M.N., Hu, X.Z., Li, Z.S., Chen, X.J., and Li, Y.Z. (2018) Competitive Interactions Between Incompatible Mutants of the Social Bacterium Myxococcus xanthus DK1622. *Front Microbiol* **9**: 1200.

Grosberg, R.K., and Strathmann, R.R. (2007) The evolution of multicellularity: A minor major

550 transition? *Annu Rev Ecol Evol S* **38**: 621-654.
551 Guo, T., Haft, D.H., and Wall, D. (2025) Myxosortase: an intramembrane protease that sorts
552 MYXO-CTERM proteins to the cell surface. *mBio*: e0406724.
553 Hodgkin, J., and Kaiser, D. (1977) Cell-to-cell stimulation of motility in nonmotile mutants of
554 *Myxococcus*. *Proc. Natl. Acad. Sci. USA* **74**: 2938-2942.
555 Jahn, R., Cafiso, D.C., and Tamm, L.K. (2024) Mechanisms of SNARE proteins in membrane
556 fusion. *Nat Rev Mol Cell Biol* **25**: 101-118.
557 Jumper, J., Evans, R., Pritzel, A., Green, T., Figurnov, M., Ronneberger, O., Tunyasuvunakool, K.,
558 Bates, R., Zidek, A., Potapenko, A., Bridgland, A., Meyer, C., Kohl, S.A.A., Ballard, A.J.,
559 Cowie, A., Romera-Paredes, B., Nikolov, S., Jain, R., Adler, J., Back, T., Petersen, S.,
560 Reiman, D., Clancy, E., Zielinski, M., Steinegger, M., Pacholska, M., Berghammer, T.,
561 Bodenstein, S., Silver, D., Vinyals, O., Senior, A.W., Kavukcuoglu, K., Kohli, P., and
562 Hassabis, D. (2021) Highly accurate protein structure prediction with AlphaFold. *Nature*
563 **596**: 583-589.
564 Kroos, L., Wall, D., Islam, S.T., Whitworth, D.E., Munoz-Dorado, J., Higgs, P.I., Singer, M.,
565 Mauriello, E.M., Treuner-Lange, A., Sogaard-Andersen, L., Kaimer, C., Elias-Arnanz, M.,
566 Stojkovic, E.A., Muller, R., Volz, C., Velicer, G.J., and Nan, B. (2025) Milestones in the
567 development of *Myxococcus xanthus* as a model multicellular bacterium. *J Bacteriol* **207**:
568 e0007125.
569 Lee, T.K., Meng, K., Shi, H., and Huang, K.C. (2016) Single-molecule imaging reveals modulation
570 of cell wall synthesis dynamics in live bacterial cells. *Nature communications* **7**: 13170.
571 Lorenzen, W., Bozhuyuk, K.A., Cortina, N.S., and Bode, H.B. (2014) A comprehensive insight
572 into the lipid composition of *Myxococcus xanthus* by UPLC-ESI-MS. *J Lipid Res* **55**: 2620-
573 2633.
574 Lucena, D., Mauri, M., Schmidt, F., Eckhardt, B., and Graumann, P.L. (2018) Microdomain
575 formation is a general property of bacterial membrane proteins and induces heterogeneity
576 of diffusion patterns. *BMC Biol* **16**: 97.
577 Morgenstein, R.M., Bratton, B.P., Nguyen, J.P., Ouzounov, N., Shaevitz, J.W., and Gitai, Z. (2015)
578 RodZ links MreB to cell wall synthesis to mediate MreB rotation and robust morphogenesis.
579 *Proc Natl Acad Sci U S A*.
580 Nan, B., Bandaria, J.N., Guo, K.Y., Fan, X., Moghtaderi, A., Yildiz, A., and Zusman, D.R. (2015)
581 The polarity of myxobacterial gliding is regulated by direct interactions between the
582 gliding motors and the Ras homolog MglA. *Proc Natl Acad Sci U S A* **112**: E186-193.
583 Nan, B., Bandaria, J.N., Moghtaderi, A., Sun, I.H., Yildiz, A., and Zusman, D.R. (2013) Flagella
584 stator homologs function as motors for myxobacterial gliding motility by moving in helical
585 trajectories. *Proc Natl Acad Sci U S A* **110**: E1508-1513.
586 Nudleman, E., Wall, D., and Kaiser, D. (2005) Cell-to-cell transfer of bacterial outer membrane
587 lipoproteins. *Science* **309**: 125-127.
588 Parry, B.R., Surovtsev, I.V., Cabeen, M.T., O'Hern, C.S., Dufresne, E.R., and Jacobs-Wagner, C.
589 (2014) The bacterial cytoplasm has glass-like properties and is fluidized by metabolic
590 activity. *Cell* **156**: 183-194.
591 Pathak, D.T., Wei, X., Bucuvalas, A., Haft, D.H., Gerloff, D.L., and Wall, D. (2012) Cell contact-
592 dependent outer membrane exchange in myxobacteria: genetic determinants and
593 mechanism. *PLoS Genet* **8**: e1002626.
594 Pathak, D.T., Wei, X., Dey, A., and Wall, D. (2013) Molecular recognition by a polymorphic cell
595 surface receptor governs cooperative behaviors in bacteria. *PLoS Genet.* **9**: e1003891.

596 Perez-Burgos, M., Garcia-Romero, I., Jung, J., Valvano, M.A., and Sogaard-Andersen, L. (2019)
597 Identification of the lipopolysaccharide O-antigen biosynthesis priming enzyme and the O-
598 antigen ligase in *Myxococcus xanthus*: critical role of LPS O-antigen in motility and
599 development. *Mol Microbiol* **112**: 1178-1198.
600 Pogue, C.B., Zhou, T., and Nan, B. (2018) PlpA, a PilZ-like protein, regulates directed motility of
601 the bacterium *Myxococcus xanthus*. *Mol Microbiol* **107**: 214-228.
602 Ramirez Carbo, C.A., Faromiki, O.G., and Nan, B. (2024) A lytic transglycosylase connects
603 bacterial focal adhesion complexes to the peptidoglycan cell wall. *Elife* **13**.
604 Rand, R.P., and Parsegian, V.A. (1984) Physical force considerations in model and biological
605 membranes. *Can J Biochem Cell Biol* **62**: 752-759.
606 Rassam, P., Copeland, N.A., Birkholz, O., Toth, C., Chavent, M., Duncan, A.L., Cross, S.J.,
607 Housden, N.G., Kaminska, R., Seger, U., Quinn, D.M., Garrod, T.J., Sansom, M.S., Piehler,
608 J., Baumann, C.G., and Kleanthous, C. (2015) Supramolecular assemblies underpin
609 turnover of outer membrane proteins in bacteria. *Nature* **523**: 333-336.
610 Rojas, E.R., Billings, G., Odermatt, P.D., Auer, G.K., Zhu, L., Miguel, A., Chang, F., Weibel, D.B.,
611 Theriot, J.A., and Huang, K.C. (2018) The outer membrane is an essential load-bearing
612 element in Gram-negative bacteria. *Nature* **559**: 617-621.
613 Sah, G.P., Cao, P., and Wall, D. (2020) MYXO-CTERM sorting tag directs proteins to the cell
614 surface via the type II secretion system. *Mol Microbiol* **113**: 1038-1051.
615 Sah, G.P., and Wall, D. (2020) Kin recognition and outer membrane exchange (OME) in
616 myxobacteria. *Curr Opin Microbiol* **56**: 81-88.
617 Shi, L., Shen, Q.T., Kiel, A., Wang, J., Wang, H.W., Melia, T.J., Rothman, J.E., and Pincet, F. (2012)
618 SNARE proteins: one to fuse and three to keep the nascent fusion pore open. *Science* **335**:
619 1355-1359.
620 Sinha, R., Ahmed, S., Jahn, R., and Klingauf, J. (2011) Two synaptobrevin molecules are sufficient
621 for vesicle fusion in central nervous system synapses. *Proc Natl Acad Sci U S A* **108**:
622 14318-14323.
623 Subedi, K., Roy, P.C., Saiz, B., Basile, F., and Wall, D. (2024) Cell-cell transfer of adaptation traits
624 benefits kin and actor in a cooperative microbe. *Proc Natl Acad Sci U S A* **121**:
625 e2402559121.
626 Sun, J., Rutherford, S.T., Silhavy, T.J., and Huang, K.C. (2022) Physical properties of the bacterial
627 outer membrane. *Nat Rev Microbiol* **20**: 236-248.
628 Tran, B.M., Punter, C.M., Linnik, D., Iyer, A., and Poolman, B. (2024) Single-protein Diffusion in
629 the Periplasm of *Escherichia coli*. *J Mol Biol* **436**: 168420.
630 van den Bogaart, G., Holt, M.G., Bunt, G., Riedel, D., Wouters, F.S., and Jahn, R. (2010) One
631 SNARE complex is sufficient for membrane fusion. *Nat Struct Mol Biol* **17**: 358-364.
632 Vassallo, C., Pathak, D.T., Cao, P., Zuckerman, D.M., Hoiczyk, E., and Wall, D. (2015) Cell
633 rejuvenation and social behaviors promoted by LPS exchange in myxobacteria. *Proc Natl*
634 *Acad Sci U S A* **112**: E2939-2946.
635 Vassallo, C.N., Cao, P., Conklin, A., Finkelstein, H., Hayes, C.S., and Wall, D. (2017) Infectious
636 polymorphic toxins delivered by outer membrane exchange discriminate kin in
637 myxobacteria. *Elife* **6**.
638 Vassallo, C.N., Sah, G.P., Weltzer, M.L., and Wall, D. (2021) Modular Lipoprotein Toxins
639 Transferred by Outer Membrane Exchange Target Discrete Cell Entry Pathways. *mBio* **12**:
640 e0238821.
641 Vassallo, C.N., Troselj, V., Weltzer, M.L., and Wall, D. (2020) Rapid diversification of wild social

642 groups driven by toxin-immunity loci on mobile genetic elements. *ISME J* **14**: 2474-2487.
643 Vassallo, C.N., and Wall, D. (2016) Tissue repair in myxobacteria: A cooperative strategy to heal
644 cellular damage. *BioEssays* **38**: 306-315.
645 Vassallo, C.N., and Wall, D. (2019) Self-identity barcodes encoded by six expansive polymorphic
646 toxin families discriminate kin in myxobacteria. *Proc. Natl. Acad. Sci. USA* **116**: 24808-
647 24818.
648 Velicer, G.J., Kroos, L., and Lenski, R.E. (2000) Developmental cheating in the social bacterium
649 *Myxococcus xanthus*. *Nature* **404**: 598-601.
650 Vlamakis, H.C., Kirby, J.R., and Zusman, D.R. (2004) The Che4 pathway of *Myxococcus xanthus*
651 regulates type IV pilus-mediated motility. *Mol Microbiol* **52**: 1799-1811.
652 Wall, D. (2014) Molecular recognition in myxobacterial outer membrane exchange: functional,
653 social and evolutionary implications. *Mol Microbiol* **91**: 209-220.
654 Wall, D., and Kaiser, D. (1998) Alignment enhances the cell-to-cell transfer of pilus phenotype.
655 *Proc Natl Acad Sci U S A* **95**: 3054-3058.
656 Wall, D., Wu, S.S., and Kaiser, D. (1998) Contact stimulation of Tgl and type IV pili in
657 *Myxococcus xanthus*. *J Bacteriol* **180**: 759-761.
658 Wei, X., Pathak, D.T., and Wall, D. (2011) Heterologous protein transfer within structured
659 myxobacteria biofilms. *Mol Microbiol* **81**: 315-326.
660 Wei, X., Vassallo, C.N., Pathak, D.T., and Wall, D. (2014) Myxobacteria produce outer membrane-
661 enclosed tubes in unstructured environments. *J Bacteriol* **196**: 1807-1814.
662 Weltzer, M.L., Guo, T., and Wall, D. (2025) Crosstalk between polymorphic toxin-immunity
663 systems involved in kin discrimination. *mBio* **0**: e00468-00425.
664 Yang, Z., Lux, R., Hu, W., Hu, C., and Shi, W. (2010) PilA localization affects extracellular
665 polysaccharide production and fruiting body formation in *Myxococcus xanthus*. *Mol*
666 *Microbiol* **76**: 1500-1513.
667 Zhang, H., Mulholland, G.A., Seef, S., Zhu, S., Liu, J., Mignot, T., and Nan, B. (2020) Establishing
668 rod shape from spherical, peptidoglycan-deficient bacterial spores. *Proc Natl Acad Sci U*
669 *S A* **117**: 14444-14452.
670 Zhang, H., Venkatesan, S., Ng, E., and Nan, B. (2023a) Coordinated peptidoglycan synthases and
671 hydrolases stabilize the bacterial cell wall. *GitHub*.
672 Zhang, H., Venkatesan, S., Ng, E., and Nan, B. (2023b) Coordinated peptidoglycan synthases and
673 hydrolases stabilize the bacterial cell wall. *Nature communications* **14**: 5357.
674 Zhou, T., and Nan, B. (2017) Exopolysaccharides promote *Myxococcus xanthus* social motility by
675 inhibiting cellular reversals. *Mol Microbiol* **103**: 729-743.

676